



Research Article

The effect of various bulbous bow forms on the resistance of a Black Sea type fishing boat

Dursun SARAL*^{id}

Department of Naval Architecture and Marine Engineering, Karadeniz Technical University, Trabzon, Türkiye

ARTICLE INFO

Article history

Received: October 07, 2024

Revised: November 19, 2024

Accepted: December 25, 2024

Key words:

Black sea type fishing boat; bulbous bow; computational fluid dynamics (CFD); resistance

ABSTRACT

In this study, resistance analyses of a 35-meter-long Black Sea Type Fishing Boat with various bow forms were conducted using Computational Fluid Dynamics (CFD). The boat's bow shapes included a normal bow without a bulb, a special bulb, a special-elliptical bulb, and an elliptical bulb. To determine the resistance values of these forms, the Realizable k- ϵ model was chosen as the turbulence model, and the Volume of Fluid (VOF) method was applied. Resistance analyses were performed at five different speeds (5.5, 7.5, 9.5, 11.5, and 13.5 knots), within the F_n range of 0.15 to 0.40. Shear, pressure, and total resistance values were presented in both tables and graphs. The CFD resistance results were compared with those from the Holtrop and Fung resistance estimation methods, and the results were found to be consistent. Performance evaluations of the bulb shapes were made by comparing the friction, pressure, and total resistance coefficients. While the special bulb resulted in the greatest reduction in total resistance, the special-elliptical bulb demonstrated better performance across a wider range of speeds. It was also concluded that the traditional elliptical bulb type is unsuitable for this type of vessel.

Cite this article as: Saral D. The effect of various bulbous bow forms on the resistance of a Black Sea type fishing boat. *Seatific* 2024;4:2:57–76.

1. INTRODUCTION

Fishing has always been an important occupation in Turkey, a country surrounded by water on three sides. Until the 1980s, fishing boats in Turkey, particularly along the Black Sea coasts, where fishing is intensively practiced, were traditionally built with wood obtained from the region's forests. With advancements in technology and the increased use of sheet metal work, steel fishing boats began to be manufactured in Turkey starting in 1975 (URL-1, 2024; URL-2, 2024). Due to their distinctive features, fishing boats built on the Black Sea coasts have come to be known as Black Sea Type Fishing Boats (Dinçer, 1992; Saral and Köse, 2024). Until the early 2000s, these boats were built without bulbs (Fig. 1), but they are now designed with bulbs (Fig. 2). Since 2002, Black Sea type fishing vessels have begun to be constructed

with bulbous bows. Due to a lack of scientific knowledge on bulbous bow applications specific to Black Sea type fishing vessels, the initial applications were implemented according to the preferences of fishing vessel owners and the knowledge and experience of shipyard craftsmen. The primary purpose of these initial applications was to counterbalance the forward trim caused by the positioning of the living quarters and the bridge at the bow by adding extra volume with a bulbous bow. Over time, vessel owners observed that ships equipped with bulbous bows could achieve higher speeds with the same engine power, indicating a reduction in form resistance. Today, bulbous bows on these types of fishing vessels are used both to correct forward trim and to reduce form resistance, thereby increasing speed. However, a comprehensive study on which type of bulbous bow is most efficient for Black Sea type fishing vessels has not yet

*Corresponding author.

*E-mail address: dursunsaral@ktu.edu.tr



been conducted. In this study, the effect of bulbous bow type on form resistance in such fishing vessels is investigated to provide insights for designers and researchers.

In shipbuilding, the bulbous bow is a crucial hydrodynamic innovation primarily designed to attenuate the wave system generated by the hull, thereby reducing total resistance and improving vessel efficiency. Its operational principle centers on generating a secondary wave system that interacts destructively with the primary wave system created by the hull. This destructive interference reduces the amplitude of the wave system, significantly diminishing wave-making resistance. By effectively dampening these waves, the bulbous bow not only minimizes energy loss to wave formation but also streamlines the water flow along the hull, reducing pressure resistance and enhancing hydrodynamic stability. This design is particularly beneficial at higher Froude numbers and for hull forms with significant wave-making components, leading to measurable improvements in fuel efficiency, reduced emissions, and optimized propulsion performance. As a result, the bulbous bow is a key feature in modern naval architecture, specifically engineered to mitigate wave resistance and maximize vessel performance.

Taylor (1923) was the first researcher to experimentally investigate the effects of bulbous bows on ship hull forms. Subsequently, experimental studies on the delta-type bulbous bow, known as the Taylor bulbous bow, were conducted by Bragg (1930), Inui et al. (1960), Ferguson (1967), and Muntjewerf (1967), systematically varying the bulbous bow parameters. Weinblum (1935), Wigley (1936), Inui (1962), and Yim (1963) conducted detailed theoretical studies on the linearized wave resistance theory. While this theory provides insights into how a bulbous bow functions, it does not offer guidance on how to design a bulbous bow for a specific hull form. Inui (1962) proposed a method for determining the size of a bulbous bow by matching the amplitude functions of the ship's forebody and the bulbous bow in regular waves. Yim (1965) established a relationship between the entrance angle at the bow and the size of the bulbous bow for a given speed. Yim (1974) presented a method consisting of three main considerations for designing spherical bulbous bows. Furthermore, Yim (1980) discussed the sheltering effect of spherical bulbous bows and proposed variations for the optimal bulbous bow position for sinusoidal, cosine, and parabolic hull types. Baba (1969) and Shearer and Steele (1970) noted that bulbous bows could provide additional benefits for ship hull forms, such as reducing wave breaking at the bow and improving flow around the keel line and bilge turn to prevent flow separation. Kracht (1978) developed a statistical method based on data obtained from propulsion model tests. This method, created by compiling data from the Hamburg and Berlin model basins, considers the block coefficient, length-to-beam ratio, and beam-to-draft ratio of the hull form. For the bulbous bow, six parameters were developed to define its size and position: width, length, depth, sectional area, lateral area, and volumetric parameters. The method provides either the power reduction achievable with a selected bulbous bow or the appropriate bulbous bow

design for a desired power reduction. The Kracht method is particularly more effective for bulbous bows with nabla (∇) cross-sections. Sharma and Sha (2005) developed a bulbous bow design method that combines two globally recognized theories: the Kracht (1978) and Yim (1980) methods. This approach optimizes bulbous bow parameters for the design speed, reanalyses the sheltering effect using approximate linear theory for resistance prediction, and statistically re-correlates existing model test results from the literature using nonlinear multivariable regression analysis. In recent years, advancements in computer technology and the widespread use of software programs have enabled the application of Computational Fluid Dynamics (CFD) to optimize hull forms with bulbous bows.

As shown in Figure 3, the three basic types of bulbous bow shapes are Delta (Δ), Circular-Elliptic (O), and Nabla (∇) (Kracht, 1978). Theories by Yim (1974) and Kracht (1978)



Figure 1. A fishing boat of the Black Sea type built in 2000 (URL-3, 2024).



Figure 2. A fishing boat of the Black Sea type built in 2019 (URL-4, 2024).

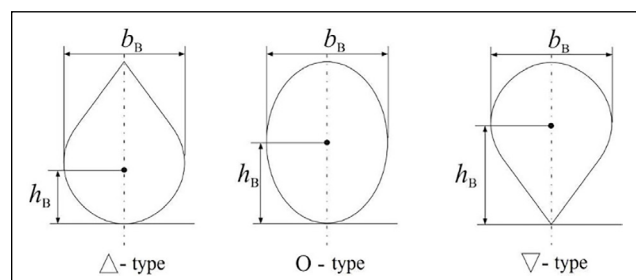


Figure 3. The sections of the bulbs (Saral et al., 2018).

are among the most accepted methods for bulb design. Additionally, specialized bulbous bow designs for specific ship hull forms are being developed.

Academic studies on fishing boats in Turkey began in 1953 with the establishment of the Ata Nutku Ship Model Testing Laboratory at Istanbul Technical University (ITU) (Saral and Köse, 2024). In Turkey, academic research on fishing vessels can be divided into three periods: first-period studies (1955-1970), ITU Fishing Boats Series studies (1979-), and Black Sea Type Fishing Boat studies (1990-) (Saral and Köse, 2024). Kafalı et al. (1979) improved the ITU Fishing Boats Series. The hull forms developed were designated as 148/1, 148/2, 148/3, 148/4, 148/5, 148/6, 148/7, 148/8, and 148/9. Resistance analyses of these generated fishing boat forms were methodically carried out at the Ata Nutku Ship Model Testing Laboratory, and none of these forms featured bulbs. A Delta (Δ) section bulb bow was added to the 148/1 form by Atlar (1977), and resistance tests on the 148/1-Y model were performed. It was determined that at a ship speed of 10.5 knots, total resistance was reduced by approximately 18%. Söylemez (1983) added three types of Delta (Δ) bulb forms, with cross-sectional area ratios of 0.12 (A1), 0.09 (A2), and 0.07 (A3), to the 148/1 model. The Kracht (1978) method was used to design the bulb forms. The resistance tests on the A1, A2, and A3 models produced the following results: The A1 model, which had the largest bulb, provided a 13% increase in effective horsepower at a service speed of 10 knots but had no effect below 9 knots. The A2 model's bulb reduced effective horsepower by 20% at a service speed of 10 knots. However, the A3 model's smaller bulb was found to be ineffective at the loaded waterline.

With the advancement of computer technologies, numerical analyses, whose foundations were first laid in the 1920s, have evolved into commercial software that became easier to use, faster, and more efficient by the 2000s (Saral, 2016). Since the 1990s, flow problems around ships have been more accurately and effectively solved using CFD software, which employs RANS equations and a variety of turbulence models (Özdemir, 2007). CFD software has been used for resistance analyses on warships with military and technical significance, followed by containers, cargo, Ro-Ro, and cargo ships with commercial importance, and most recently, on today's fishing vessels. Below are some academic studies that explore the calculation of resistance using CFD on fishing vessel forms. Setyawan et al. (2010) investigated the multi-hull form using CFD to reduce fuel consumption in fishing vessels. Samuel et al. (2015) used CFD to analyze the resistance of a single-hull fishing boat from Indonesia's Cilacap region, as well as the catamaran created from the same hull. Li et al. (2016) modeled a tuna longline fishing boat and conducted both model resistance experiments and resistance analyses using CFD. Additionally, resistance analyses were performed using CFD by systematically changing the bulb size on the ship. When the total resistance values of the new bulb forms were compared, it was found that the 50% elongated bulb form reduced total resistance by around 5%. Abramowski and Sugalski (2017) examined nine Polish fishing vessels and applied cylindrical (O) and

nabla (∇) type bulb forms to two selected designs. CFD was used to perform resistance analyses on these forms. When the total resistance values were compared, it was found that the cylindrical (O) type bulb reduced total resistance by 14%, while the nabla (∇) type bulb reduced total resistance by 16%. Kim et al. (2018) conducted CFD analyses on a traditional catamaran fishing boat from the Cilacap region of Indonesia, applying delta (Δ), nabla (∇), and elliptical (O) type bulbs. The analysis showed that the nabla (∇) type bulb reduced the total resistance of the fishing boat by about 10% at service speed. Bahatmaka and Kim (2019) used CFD to analyze the resistance of two traditional Indonesian fishing boats operating in the north and south of Java Island. The analysis indicated that the fishing boats used in the southern region were more suitable in terms of resistance. Raju et al. (2020) added delta (Δ), nabla (∇), and elliptical (O) bulb forms to a traditional tuna longline vessel. CFD was used to perform resistance analyses on these forms in calm water. The results showed that the elliptical (O) bulb form had 5.35% lower total resistance compared to the form without a bulb. In Tran et al. (2021) study, a new bulbous bow design method that goes beyond traditional Kracht charts is presented. The study optimizes power reduction by resizing the initial design from Kracht charts using a multi-objective function combined with CFD analysis and surrogate models. Applied to the FAO 75 fishing vessel, this method achieved approximately 14% power savings, with results aligning well with theoretical expectations. In Szelangiewicz et al. (2021) study, the impact of adding a simple-shaped bulbous bow as a low-cost retrofit to reduce environmental impact on older fishing vessels is examined. The study's CFD analyses show significant reductions in resistance, fuel consumption, and greenhouse gas emissions in vessels equipped with a bulbous bow. These findings highlight potential environmental and economic benefits, particularly for older fishing vessels modernized at low cost. In Iqbal et al. (2021) study, the use of a foil-shaped center bulb to reduce total resistance in catamaran fishing vessels is examined. The study tested six different bulb configurations using the CFD method and found that Model 6, where the center bulb length was increased by 15% and width and height reduced by 10%, provided the best results. This model achieved a 10.68% reduction in resistance. In Díaz Ojeda et al. (2023) study, the importance of optimizing ship lines to reduce environmental impact and improve operational efficiency is highlighted. The study compares the numerical analysis and towing tank experiments of two fishing vessel hulls, demonstrating a reduction in resistance of over 10% with the addition of a dihedral bulbous bow. This bow structure is noted to reduce pressure resistance by smoothing the flow reaching the bow. In Oyuela et al. (2024) study, the hydrodynamics of a typical Argentinian fishing vessel in calm water were analyzed, with an evaluation of total resistance components at various draft conditions. The study uses experimental data from the University of Buenos Aires towing tank, analyzed with the 1978 ITTC Power Prediction method and validated through numerical studies conducted with OpenFOAM

V10. The resulting numerical model discusses the potential for improving total force prediction by combining EFD results with the CFD form factor. In the study by Diaz Ojeda et al. (2024), the effect of the bulbous bow design, used in naval hydrodynamics to reduce resistance, is examined. The study evaluates a typical Argentinian trawler fishing vessel by comparing configurations with and without the bulbous bow under different load conditions and speeds. Numerical analyses were conducted using OpenFOAM, and the results were validated through towing tank experiments.

CFD studies on Turkish-type fishing vessels are as follows. A CFD application for the ITU Fishing Boats Series was performed by Saral et al. (2018). CFD analyses were conducted on the 148/3, 148/4, 148/8, and 148/9 coded boat forms. Delta (Δ), Nabla (∇), and Elliptical (O) shaped bulbous bows were applied to these forms to evaluate the effectiveness of the bulb shapes. The effectiveness of the bulbs at a service speed of 10 knots was determined to be 10% for boats with a block coefficient of 0.405 and 13% for boats with a block coefficient of 0.495. Saral and Köse (2020) used CFD to analyze the resistance of a Black Sea-type fishing boat in calm water at speeds ranging from 1 to 15 knots (F_n 0.028–0.420). The economic service speed of Black Sea-type fishing boats was determined by CFD analysis to be 11 knots. In Saral (2023) study, a dimensionless offset table was developed to optimize and standardize the "Black Sea Type Fishing Vessel" (KTBG) forms for vessels between 40–60 meters in length.

Using StarCCM+ CFD software, resistance values of various KTBG forms were calculated, and the effects of different bow, stern, and skeg designs on resistance were examined. The study indicates that KTBG standard dimensionless offset table forms exhibit improved resistance characteristics.

The objective of this study is to identify the most effective type of bulbous bow in reducing total resistance for Black Sea-type fishing vessels with a length of 35 meters (ranging between 30–40 meters). To achieve this, resistance analyses were conducted under calm water and stationary conditions for the following configurations: the existing fishing vessel form (Form SB), the bulbous bow-less version of this form (Form WB), the elliptical bulbous bow form developed for ITU fishing boats series (Form EB), and a custom elliptical bulbous bow form (Form SBE) that incorporates characteristics of the own bulbous bow and the elliptical bulbous bow. Resistance analyses of the boat forms were conducted using CFD. To evaluate the efficiency of the special bulb, resistance analyses of the form without the bulb were also performed. The elliptical bulb, one of the bulbs used, is based on the optimum elliptical bulb form developed by Saral et al. (2018) for the ITU fishing boats series. The other bulb form is a new special elliptical bulb created by combining the special and elliptical bulb designs. All CFD analyses on the hull forms were performed using the Hull Performance Workflow module of the StarCCM+ software. In these CFD analyses, the Realizable k - ϵ Model

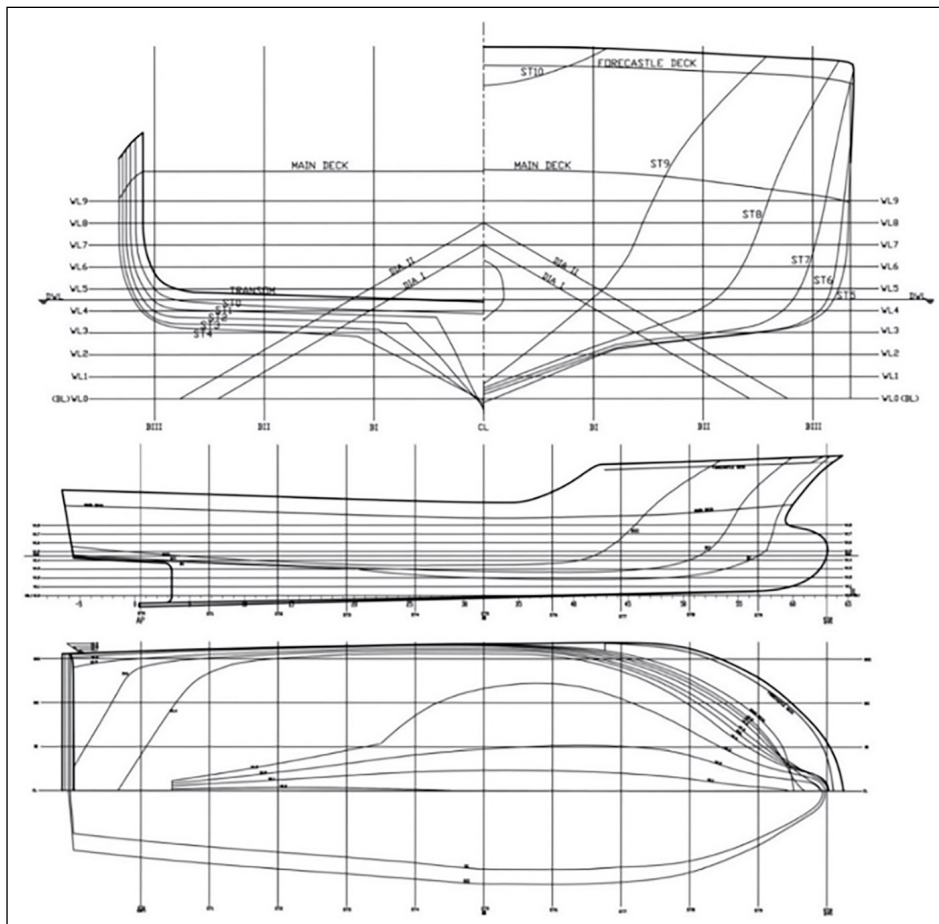


Figure 4. Form SB lines plan (Saral and Köse, 2020).

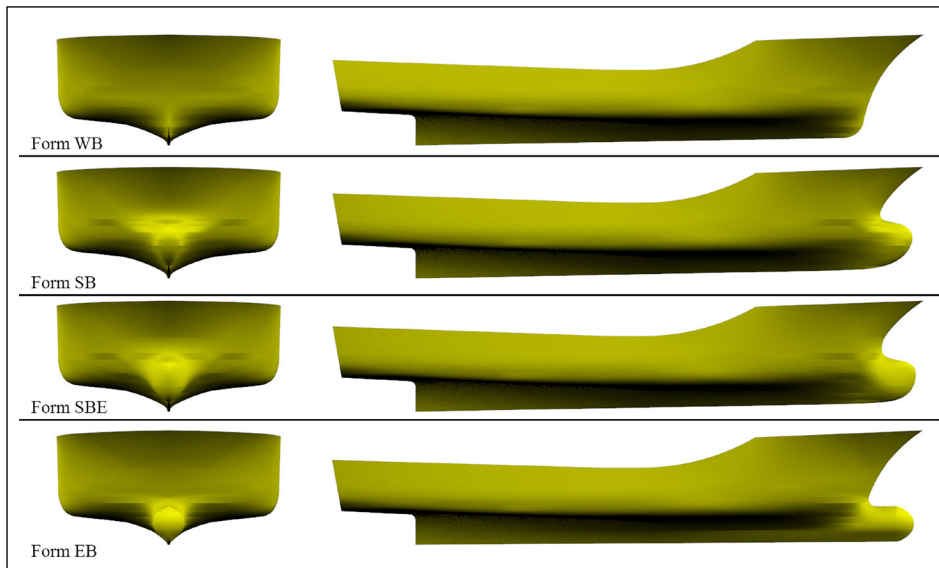


Figure 5. Body and profile views of the three-dimensional forms.

WB: Without Bulb Form; SB: Special Bulb Form; EB: Elliptical Bulb Form

was used as the turbulence model, and the VOF method was applied. Resistance tests were conducted in the F_n 0.15 to F_n 0.40 range at five different speeds (5.5, 7.5, 9.5, 11.5, and 13.5 knots). The total resistance values of the boat forms were compared to determine which head form is most suitable for the Black Sea-type fishing vessels with a length of approximately 35 meters.

2. FISHING BOATS GEOMETRICAL CHARACTERISTICS

In this study, four Black Sea-type fishing vessel forms with an overall length of 35.60 meters and a beam of 13.32 meters (at the main deck) were analyzed. The main form (Fig. 4) used in this study is a typical Black Sea-type fishing vessel constructed at the Yeniay-Çamburnu shipyards (Sürmene-Trabzon), which was previously subjected to resistance analysis using CFD in the speed range of 1-15 knots by Saral and Köse (2020). The other three forms were designed based on this form.

In the article, the forms are named as follows to facilitate tracking of the vessels: Form WB for the bulb-less version, Form SB for the special bulb version, Form SBE for the special elliptical bulb version, and Form EB for the elliptical bulb version.

The body plan of the existing vessel form, Form SB, is provided in Figure 4. The bulbous bow on Form SB was designed based on the preferences of fishing vessel owners and the knowledge and experience of shipyard craftsmen. Academic knowledge was not utilized in determining the dimensions and shape of the bulbous bow. In Black Sea-type fishing vessels, the reason for designing bulbous bows with half of their structure above the design waterline is to balance the forward trim caused by the placement of living quarters and the bridge at the bow.

Form WB is the bulb-less form, developed from Form SB by referencing bulb-less Black Sea-type fishing vessels.

Form EB is the elliptical bulbous bow form. The dimensions and shape of the elliptical bulbous bow were developed using the dimensionless offset values provided by Saral et al. (2018) for the ITU Fishing Vessel series forms. It was selected because it demonstrated the best performance in the ITU Fishing Vessel series.

Form SBE is the special elliptical bulbous bow form. It was created by combining the dimensions of the bulbous bow from Form SB with the dimensionless semi-width offset values of the elliptical bulbous bow from Form EB.

The three-dimensional versions of all forms were created using Rhino software. The body and profile views of the three-dimensional forms are presented in Figure 5.

The frames of the analysed forms between stations 8 and 10 differ depending on the shape of the bulbous bow. The comparison of the changes in bulbous bow shapes in the profile view is presented in Figure 6, while

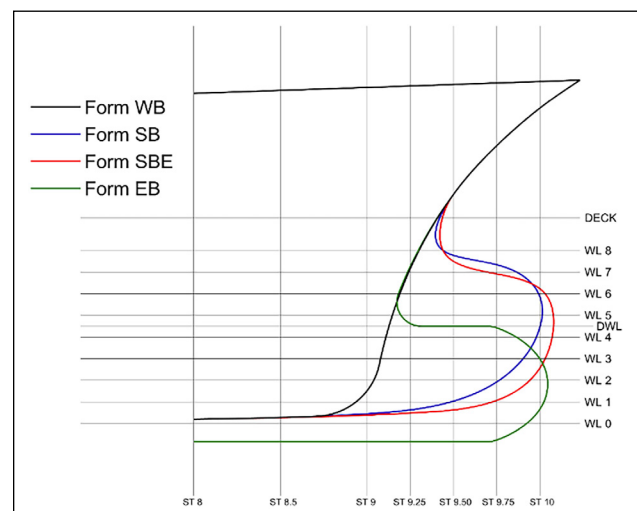


Figure 6. Comparison of the stem profiles of the forms in the profile plan.

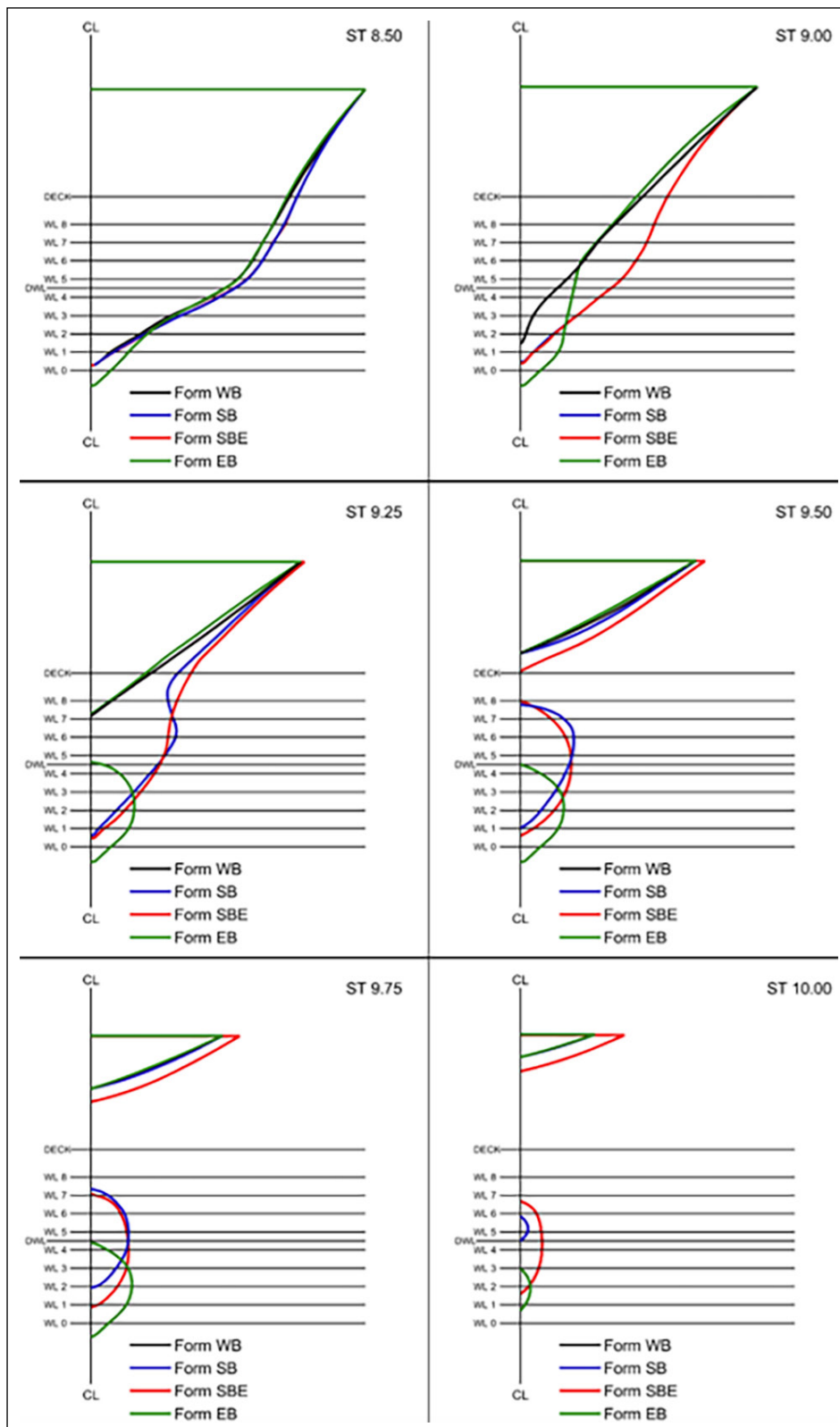


Figure 7. Comparison of the frames of the forms between stations 8 and 10 in the body plans.

the comparison of the changes in the frames between stations 8 and 10 is shown in Figure 7.

In the CFD resistance analyses, it is assumed that the forms have the same displacement value. The fixed displacement value for the forms is 394.313 tons, which corresponds to the displacement of the vessels at their waterline during

fishing operations (with full fuel and water tanks, nets on the aft deck, and empty fish holds). The displacement values of the forms were calculated using the weight and volume estimation formulas for Black Sea-type fishing vessels developed by Saral (2023). However, the displacement value of the bulb-less form is approximately

Table 1. Geometric features of boat forms computed using Hull Performance Workflow

Main particular	Symbol	Unit	Form WB	Form SB	Form SBE	Form EB
Length at the waterline	L_{WL}	m	31.808	34.440	34.598	31.863
Length overall	L_{OA}	m	35.580	35.578	35.580	35.569
Beam	B	m	13.125	13.112	13.112	13.098
Draught	T	m	2.542	2.542	2.526	2.586
Displacement (volume)	∇	m^3	380.533	384.494	384.757	384.147
Displacement (mass)	Δ	ton	390.251	394.313	394.583	393.957
Static hull wetted surface	S	m^2	429.610	440.966	442.253	452.013
Block coefficient	C_B	-	0.359	0.335	0.336	0.356
Prismatic coefficient	C_P	-	0.724	0.669	0.664	0.751

WB: Without Bulb Form; SB: Special Bulb Form; SBE: Special Elliptical Bulb Form; EB: Elliptical Bulb Form.

Table 2. The velocity and Fn values at which CFD analyses are performed

Velocities	Velocities tested	Unit	Form WB Fn	Form SB Fn	Form SBE Fn	Form EB Fn
5.5 knots	2.829	m/s	0.160	0.154	0.154	0.160
7.5 knots	3.858	m/s	0.218	0.210	0.209	0.218
9.5 knots	4.887	m/s	0.277	0.266	0.265	0.276
11.5 knots	5.916	m/s	0.335	0.322	0.321	0.335
13.5 knots	6.944	m/s	0.393	0.378	0.377	0.393

WB: Without Bulb Form; SB: Special Bulb Form; SBE: Special Elliptical Bulb Form; EB: Elliptical Bulb Form.

4 tons less than the other forms, corresponding to the weight of the bulbous bow.

The properties of the forms, as calculated by the Hull Performance Workflow after incorporating the ship forms into the software, are listed in Table 1. Upon examining Table 1, it can be observed that the draft values of the forms vary to maintain the same displacement. The variation in draft values also leads to changes in the waterline length of the forms. This, in turn, causes differences in the Froude numbers (Fn) of the forms at the speed values specified for the resistance analyses. The Froude numbers of the forms at the analyzed speed values are presented in Table 2.

3. NUMERICAL MODELLING

3.1. Theoretical equations

In this study, the theoretical equations governing fluid flow are solved using the Unsteady Reynolds-Averaged Navier-Stokes (URANS) methodology, which is widely employed for analyzing unsteady and turbulent flows. The URANS approach involves time-averaging the Navier-Stokes equations to capture the mean flow behavior while accounting for transient flow phenomena and turbulent fluctuations through appropriate turbulence models. This method is particularly effective for simulating complex flow patterns around ship hulls, including wave formation and flow separation.

The governing equations, which represent the principles of mass and momentum conservation, are solved numerically using the Computational Fluid Dynamics (CFD) software STAR-CCM+.

For incompressible flows, the time-averaged continuity equation and momentum equation are expressed in tensor notation and Cartesian coordinates, as presented in Equations (1) and (2). The continuity equation ensures mass conservation, while the momentum equation accounts for the effects of pressure, viscous forces, and unsteady flow terms. These equations form the mathematical foundation for the simulations, enabling the detailed analysis of hydrodynamic resistance, flow characteristics, and wave patterns around the hull under investigation.

$$\frac{\partial(\rho \bar{u}_i)}{\partial x_i} = 0 \quad (1)$$

$$\frac{\partial(\rho \bar{u}_i)}{\partial t} + \frac{\partial}{\partial x_i} (\rho \bar{u}_i \bar{u}_j + \rho \overline{u'_i u'_j}) + \frac{\partial \bar{p}}{\partial x_i} + \frac{\partial(\rho \bar{\tau}_{ij})}{\partial x_j} \quad (2)$$

where ρ is density, \bar{u}_i is the averaged Cartesian components of the velocity vector, $\rho \overline{u'_i u'_j}$ is the Reynolds stresses and \bar{p} is the mean pressure. $\bar{\tau}_{ij}$ is the mean viscous stress tensor components, as shown in equation (3).

$$\bar{\tau}_{ij} = \mu \left(\frac{\partial \bar{u}_i}{\partial x_j} + \frac{\partial \bar{u}_j}{\partial x_i} \right) \quad (3)$$

in which μ is the dynamic viscosity.

3.2. Model of turbulence

The Realizable $k-\varepsilon$ model was selected to calculate the resistance of the forms. The Hull Performance Workflow module of the StarCCM+ software specializes in calculating ship resistance using the Realizable $k-\varepsilon$ model (Siemens,

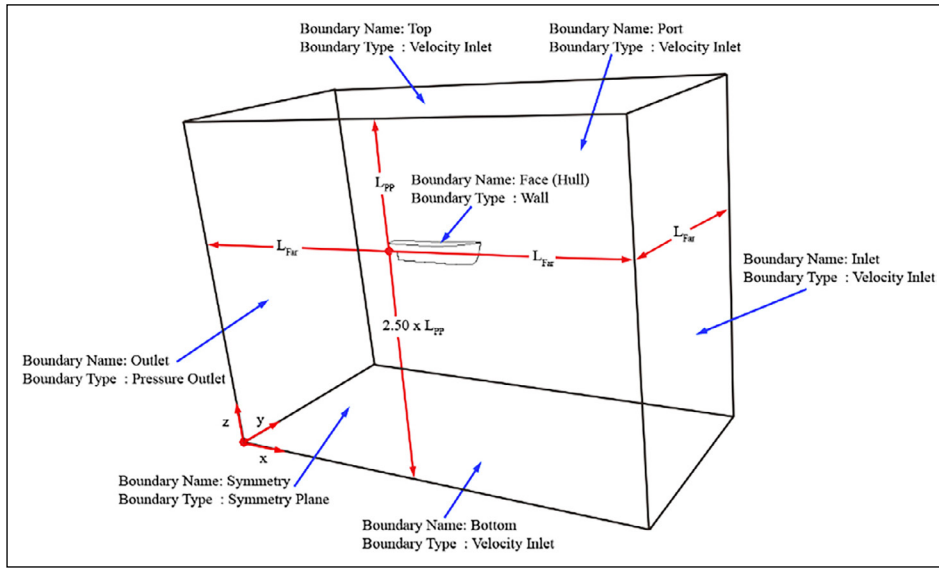


Figure 8. Computational domain dimensions and boundary conditions.

2021). Therefore, this turbulence model was chosen to calculate the resistance of the forms.

The "Realizable k - ϵ Model," developed by Shih et al. (1995), is the most advanced version of the k - ϵ model.

There are two basic differences from the standard k - ϵ model. The first is that the model contains a new transport equation for the turbulence loss rate ϵ . Second, C_{μ} , a critical coefficient of the model, is expressed as a function of the mean flow and turbulence properties rather than being fixed as in the standard model. The understanding of an C_{μ} variable is also compatible with the experimental data in boundary layer.

Shih et al. (1995) developed transport equations (equations (4) and equations (5)) are as follows:

$$\frac{\partial}{\partial t}(\rho k) + \frac{\partial}{\partial x_j}(\rho k u_j) = \frac{\partial}{\partial x_j} \left[\left(\mu + \frac{\mu_t}{\sigma_k} \right) \frac{\partial k}{\partial x_j} \right] + G_k + G_b - \rho \epsilon - Y_M + S_K \quad (4)$$

$$\frac{\partial}{\partial t}(\rho \epsilon) + \frac{\partial}{\partial x_i}(\rho \epsilon u_i) = \frac{\partial}{\partial x_j} \left[\left(\mu + \frac{\mu_t}{\sigma_\epsilon} \right) \frac{\partial \epsilon}{\partial x_j} \right] + \rho C_1 S_\epsilon - \rho C_2 \frac{\epsilon^2}{k + \sqrt{v \epsilon}} + C_{1\epsilon} \frac{\epsilon}{k} C_{3\epsilon} G_b + S_\epsilon \quad (5)$$

In this equation G_k is the production of turbulent kinetic energy due to average velocity gradients, G_b is the production of turbulence kinetic energy as a result of temperature differences in density, Y_M is constrictive turbulence depicts the effect of turbulence expansion on the entire spread. The terms S_K and S_ϵ are user-defined source terms.

4. NUMERICAL PROCEDURE

All CFD analyses of the hull forms were conducted using the Hull Performance Workflow (HPW) module in the StarCCM+ software.

The HPW module in StarCCM+ is designed for analyzing displacement hulls without appendages and provides a user-friendly interface for simulations under calm water conditions. It adheres to industry standards, managing critical aspects such

as geometric domain definition, mesh refinement, transient simulation settings, and wave damping, ensuring accurate and reliable completion of CFD analyses (Siemens, 2021).

The forms were modeled in three dimensions using the Rhinoceros software and converted to IGS format. Using the HPW module, the IGS-format forms were imported into the Star-CCM+ program, and a computational domain representing a virtual towing tank was created around the boat geometry (Fig. 8).

The names and boundary conditions of the virtual towing tank's boundary surfaces are defined as shown in Figure 8.

The dimensions of the computational domain are determined automatically and are proportional to the length between perpendiculars (L_{PP}) of the hull. Equation (6) defines the L_{Far} parameter as a function of the Froude number and wake wavelengths (Siemens, 2021).

Farfield distance from the hull (L_{Far}):

$$L_{Far} = L_{Dmax} + L_{Bmax} \quad (6)$$

Maximum damping length (L_{Dmax}):

$$L_{Dmax} = 4.5e^{-3.75 \cdot Fn} \cdot \lambda_{max} \quad (7)$$

Maximum buffer length (L_{Bmax}):

$$L_{Bmax} = 0.4925 \cdot Fn^{-0.8} \cdot \lambda_{max} \quad (8)$$

Wake wavelength at maximum allowed ship speed (λ_{max}):

$$\lambda_{max} = \frac{2\pi}{g} \cdot V_{Smax}^2 \quad (9)$$

Maximum allowed ship speed (V_{Smax}):

$$V_{Smax} = 0.4 \cdot \sqrt{g L_{WL}} \quad (10)$$

Froude number (Fn):

$$Fn = \frac{V_s}{\sqrt{g \cdot L_{WL}}} \quad (11)$$

Where L_{WL} is waterline length, V_s is ship speed, g is acceleration due to gravity.

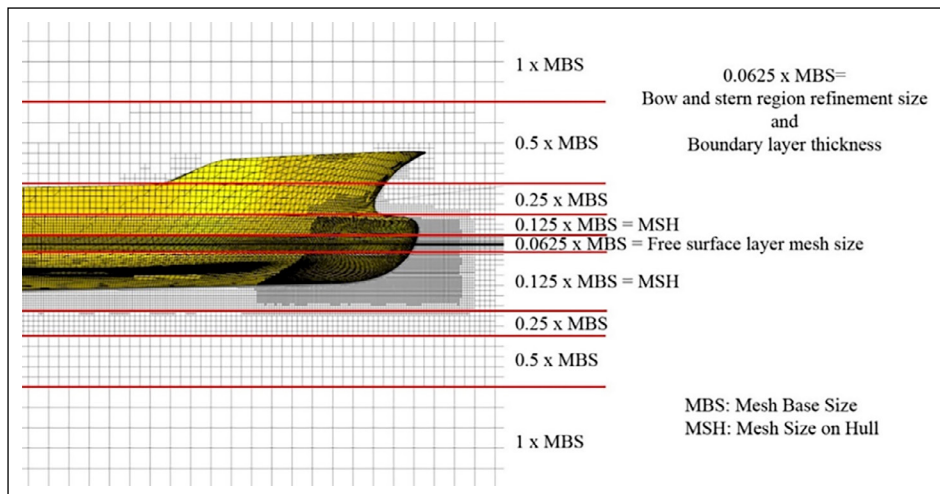


Figure 9. Cell size variation of the volume mesh structure and cell dimensions according to MBS.

MBS: Mesh base size; MSH: Mesh size on the hull.

For each CFD resistance analysis, the HPW automatically generated the volume mesh structure using the surface remesher, trimmed cell mesher, and prism layer mesher tools, resulting in the creation of three-dimensional hexahedral cells. The mesh base size (MBS) was calculated by dividing the LPP values of the forms by a specified denominator, as described in Equation (12). Based on the determined MBS, the mesh size on the hull (MSH) was calculated using Equation (13). Equation (14) was applied to calculate the cell sizes for the free surface layer, boundary layer thickness (BLT), and the refinement size in the bow and stern regions.

Figure 9 illustrates the variation in cell sizes of the volume mesh structure used in CFD resistance analyses, depending on changes in the mesh base size (MBS) and cell dimensions.

$$MBS = \frac{L_{pp}}{\text{Denominator}} \quad (12)$$

$$MSH = \frac{12.5}{100} MBS \quad (13)$$

$$BLT = \frac{6.25}{100} MBS \quad (14)$$

The HPW automatically configures the y^+ and Δs values based on the specific characteristics of the problem being analyzed. Typically, HPW sets the y^+ value to 30; however, variations in the vessel's geometry may cause the y^+ value to occasionally deviate above or below this target. These fluctuations have minimal impact on the overall solution accuracy due to the use of a blended wall function. The boundary layer thickness is represented by 6 to 9 cells, depending on the BLT value, with an expansion ratio of 1.5.

The HPW generates a mesh of volumes around the hull and on the free surface using automatic volumetric refinement. The positions and sizes of these refinements are determined according to industry standards to ensure a high degree of accuracy while maintaining a low cell count. There are three volumetric refinements used to resolve the free surface, and

these refinements are sized to approximately match the water stagnation height at $Fn = 0.15, 0.275,$ and 0.4 in the vertical direction (Siemens, 2021).

The body, profile, and waterline (free surface) plane views of the volume mesh structure created for the forms are shown in Figure 10.

The mesh properties of the virtual towing tank, generated by HPW based on the selected denominator value, along with the mesh solution times and computer processor specifications, are presented in Table 3. The mesh structures for the forms are shown in Figure 11.

Additionally, the mesh structures in the bow and stern regions of the forms are shown in Figures 12 and 13, respectively, for a closer view.

Once the volume mesh structures were generated, the physical models required for hull resistance analysis in HPW were automatically configured under calm water conditions, as illustrated in Figure 14. For the CFD resistance analyses, the hull forms were treated as fixed, with no adjustments made for trim or sinkage. To optimize computational efficiency, a half-model approach was utilized during the simulations. The CFD resistance analyses were conducted at full scale for the ship's dimensions.

The physical runtime of the simulation is determined automatically. The Hull Performance Workflow monitors the hull's average resistance at each speed. The run terminates if the average resistance fluctuates by less than 0.5 percent over the preceding 500 time steps. If the stopping criterion is not met, the simulation terminates after a maximum of 7500 time steps for the initial hull speed and 3,500 time steps for each subsequent hull speed (Siemens, 2021).

5. MESH DEPENDENCY STUDY

The validation and uncertainty assessment of the CFD resistance analyses was conducted in accordance with the

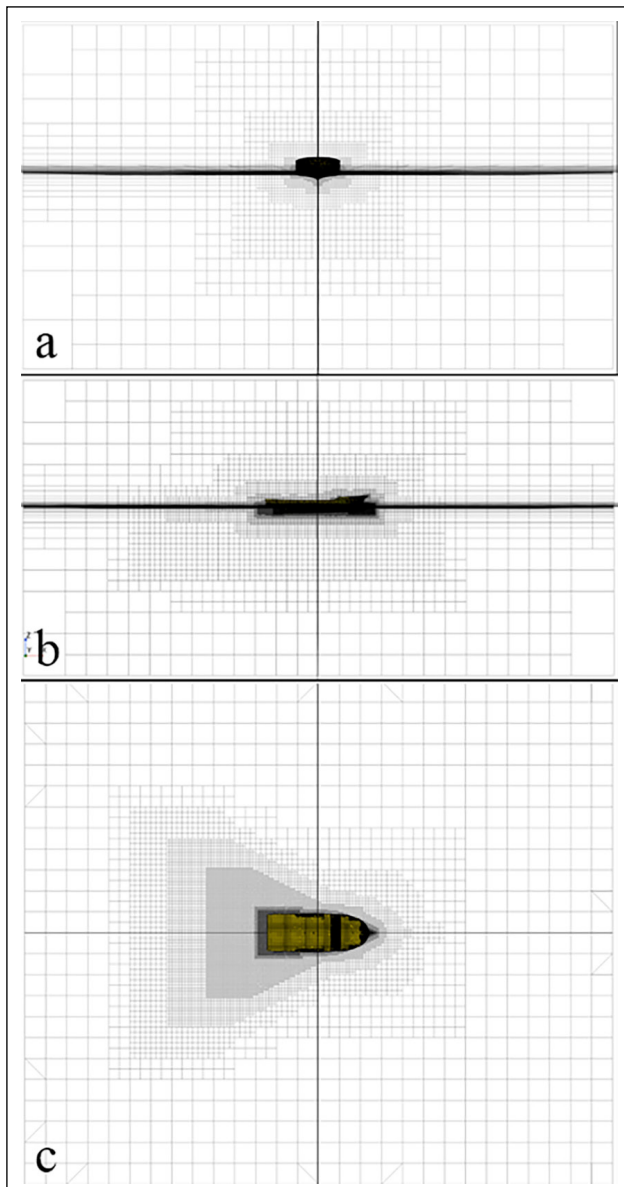


Figure 10. Body (a), profile (b), and waterline (free surface) plane (c) views of the volume mesh.

ITTC (2021) procedure. In the study, a refinement ratio of $\sqrt{2}$ was adopted, and coarse, medium, and fine mesh structures were generated based on the MSH value of Form SB. The properties of the mesh structures created for the analyses and the CFD analysis durations are provided in

Table 4, while the total resistance values obtained from the CFD analyses are presented in Table 5.

To assess uncertainty, the Grid Convergence Index (GCI) was utilized, following the proposal by Roache (1994) and in accordance with the ITTC (2021) procedure. The GCI utilizes a grid refinement error estimator based on the generalized Richardson (1927) extrapolation principles. This estimator serves as a robust tool for evaluating the uncertainty associated with grid convergence in an asymptotic setting.

The GCI calculations, based on the total resistance values of Form SB for coarse, medium, and fine grids, are presented in Figure 15. A closer examination of these computations reveals that monotonic convergence is consistently observed across all CFD resistance analyses conducted in this study. This consistent pattern reinforces the reliability and accuracy of the analytical methodology, thereby validating the robustness of the conclusions drawn.

6. RESULTS AND DISCUSSIONS

The results of the CFD resistance analyses conducted on the ship forms are presented in Tables 6, 7, 8, and 9 for Forms WB, SB, SBE, and EB, respectively.

To demonstrate the accuracy of the resistance values derived from the CFD analyses, the forms were modeled using the Maxsurf Modeler program, and the resistance analyses were performed with the Maxsurf Resistance program using the Holtrop and Fung resistance estimation methods. A comparison of the effective power values found by CFD and those estimated by the Holtrop and Fung methods is shown in Figures 16, 17, 18, and 19 for Form WB, Form SB, Form SBE, and Form EB, respectively. The total resistance values found by CFD for each form fall between the total resistance curves estimated by Holtrop and Fung, as seen in Figures 16, 17, 18, and 19. In the Maxsurf Resistance program, when calculating the effective power values, the efficiency for the Fung method was assumed to be 100%. For the Holtrop method, efficiency values of 95%, 80%, 69%, 67%, and 63% were assumed for speeds of 5.5, 7.5, 9.5, 11.5, and 13.5 knots, respectively. These values were derived by subtracting the values obtained from dividing Pressure Resistance by Total Resistance from the values obtained by dividing Shear

Table 3. Mesh properties of the virtual towing tank, mesh solution times, and computer properties

	Unit	Form WB	Form SB	Form SBE	Form EB
LBP	m	28.767	31.393	31.559	28.792
Denominator		35	35	35	35
Mesh base size	m	0.822	0.897	0.902	0.823
Mesh size on hull	m	0.103	0.112	0.113	0.103
Mesh cell count	m	1,556,187	1,423,762	1,413,366	1,557,309
Total runtime	s	86449	78709	84600	84500
# of Processors			2×Intel Xeon E5 2667 (16×3.30 GHz)		

WB: Without Bulb Form; SB: Special Bulb Form; SBE: Special Elliptical Bulb Form; EB: Elliptical Bulb Form; LBP: Length Between Perpendiculars.

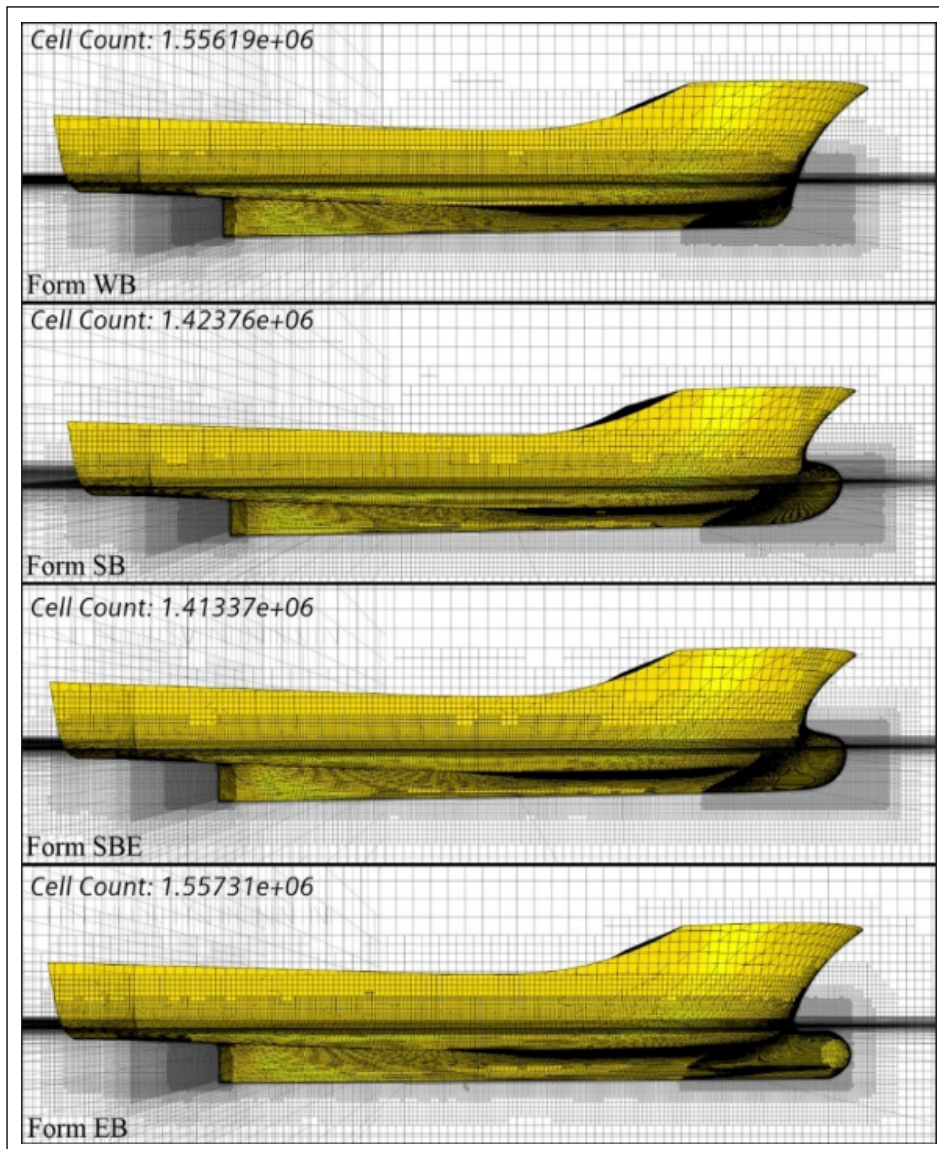


Figure 11. The mesh structures for the forms.

WB: Without Bulb Form; SB: Special Bulb Form; SBE: Special Elliptical Bulb Form; EB: Elliptical Bulb Form.

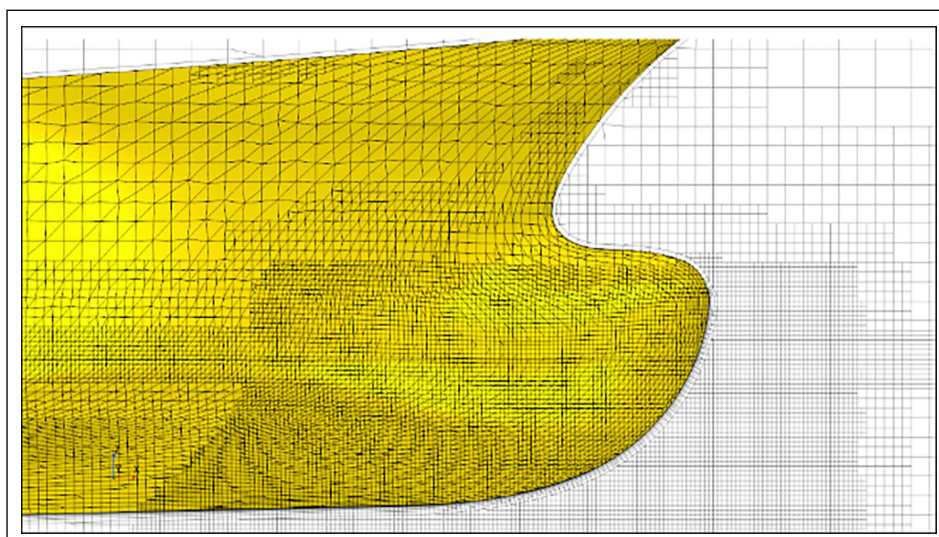


Figure 12. The view of the mesh structure on the bow form of the vessel in the profile plane.

Table 4. Properties of computational domains created according to denominators for the Form SB and solution times of CFD analyses

Ship code	L _{OA} (m)	L _{pp} (m)	Denominator	MBS (m)	MSH (m)	Mesh cell count	Total runtime	
							(sec)	(hour)
Form SB-coarse grid	35.578	31.393	24.8	1.269	0.158	661,907	36591	10.16
Form SB-medium grid	35.578	31.393	35.0	0.897	0.112	1,423,762	78709	21.86
Form SB-fine grid	35.578	31.393	49.6	0.634	0.079	3,181,538	175883	48.85

SB: Special Bulb Form; CFD: Computational Fluid Dynamics; L_{OA}: Length Overall; L_{pp}: Length Between Perpendiculars; MBS: Mesh base size; MSH: Mesh size on the hull.

Table 5. Total resistance values obtained from CFD resistance analysis of Form SB for mesh independence

Velocity		Fn	Form SB-coarse grid	Form SB-medium grid	Form SB-fine grid
(knots)	(m/s)		RT (kN)	RT (kN)	RT (kN)
5.5	2.829	0.154	8.857	8.662	8.612
7.5	3.858	0.210	18.246	17.398	17.117
9.5	4.887	0.266	33.187	32.518	32.408
11.5	5.916	0.322	64.107	62.906	62.657
13.5	6.944	0.378	119.126	117.100	116.632

CFD: Computational Fluid Dynamics; SB: Special Bulb Form; RT: Total Resistance.

Resistance by Total Resistance, and then subtracting the result from 1. Thus, the effective power values account for the power losses caused by the Holtrop method's inability to fully calculate wave resistance at higher speeds.

From the graphs, it can be observed that the CFD results for Form WB and Form EB closely match the Holtrop results. However, for Forms SBE and SB, the Holtrop results fall below the CFD results after a speed of 11 knots. This is due to the wave rising above the bulbous bow at 11 knots, causing the bulbous bow to submerge and creating additional frictional and pressure resistance. The Holtrop method in the Maxsurf Resistance program is unable to account for this effect. Considering all these calculations, the total resistance values obtained from the CFD are within acceptable ranges.

The comparison graphs for the frictional resistance coefficient (C_F), the pressure resistance coefficient (C_p) and the total resistance coefficient (C_T), are shown in Figures 20, 21, and 22, respectively. To equalize the displacement values of the ships, it was necessary to adjust their draft values. Changing the draft values altered the waterlines (L_{wl}) at which the ships float, and consequently, the Froude numbers (Fn) for the same speed values also changed. As a result, different Fn values were obtained for the same speed values. The CF, CP, and CT values were plotted in the graphs as functions of Fn. The points on the curves in the graphs represent the speeds of 5.5, 7.5, 9.5, 11.5, and 13.5 knots in order from the origin outward.

As can be seen in Figure 20, as the Froude number increases, the C_F values decrease for all forms, indicating the typical behavior of frictional resistance. This is expected because frictional resistance diminishes with higher speeds relative to the boundary layer effects. Form WB has the highest C_F

across most Fn values, indicating that the bulb-less form generates higher frictional resistance due to the absence of a streamlined bulbous bow to smooth water flow. Form SB and Form SBE exhibit similar trends, but lower C_F values compared to Form WB. This suggests that the addition of a bulbous bow reduces frictional resistance. Between these two, Form SB generally performs better, showing the lowest C_F values at most Fn values. Form EB shows moderate performance compared to the others, with C_F values slightly higher than Form SBE but generally lower than Form WB and sometimes Form SB. Form SB demonstrates the best performance in terms of frictional resistance reduction across most Fn values, followed closely by Form SBE. There are points where the lines intersect, indicating that at specific Fn values, the relative performance of the forms changes. This suggests that the efficiency of the bulbous bow design may vary depending on the operational speed (represented by Fn). In summary, Form WB consistently exhibits the highest frictional resistance, making it the least efficient. The addition of bulbous bows (SB, SBE, EB) improves hydrodynamic performance, with Form SBE being the most effective in reducing frictional resistance, especially at higher Fn values. The results emphasize the importance of bulbous bow design in minimizing resistance and improving efficiency, particularly for higher-speed ranges.

As can be seen in Figure 21, across all forms, C_p increases as Fn rises. This is expected, as higher Fn values correspond to increased wave-making resistance, which is a significant component of pressure resistance. Form WB exhibits relatively higher C_p values compared to other forms at most Fn values, especially at higher Froude numbers. This indicates that the absence of a bulbous bow

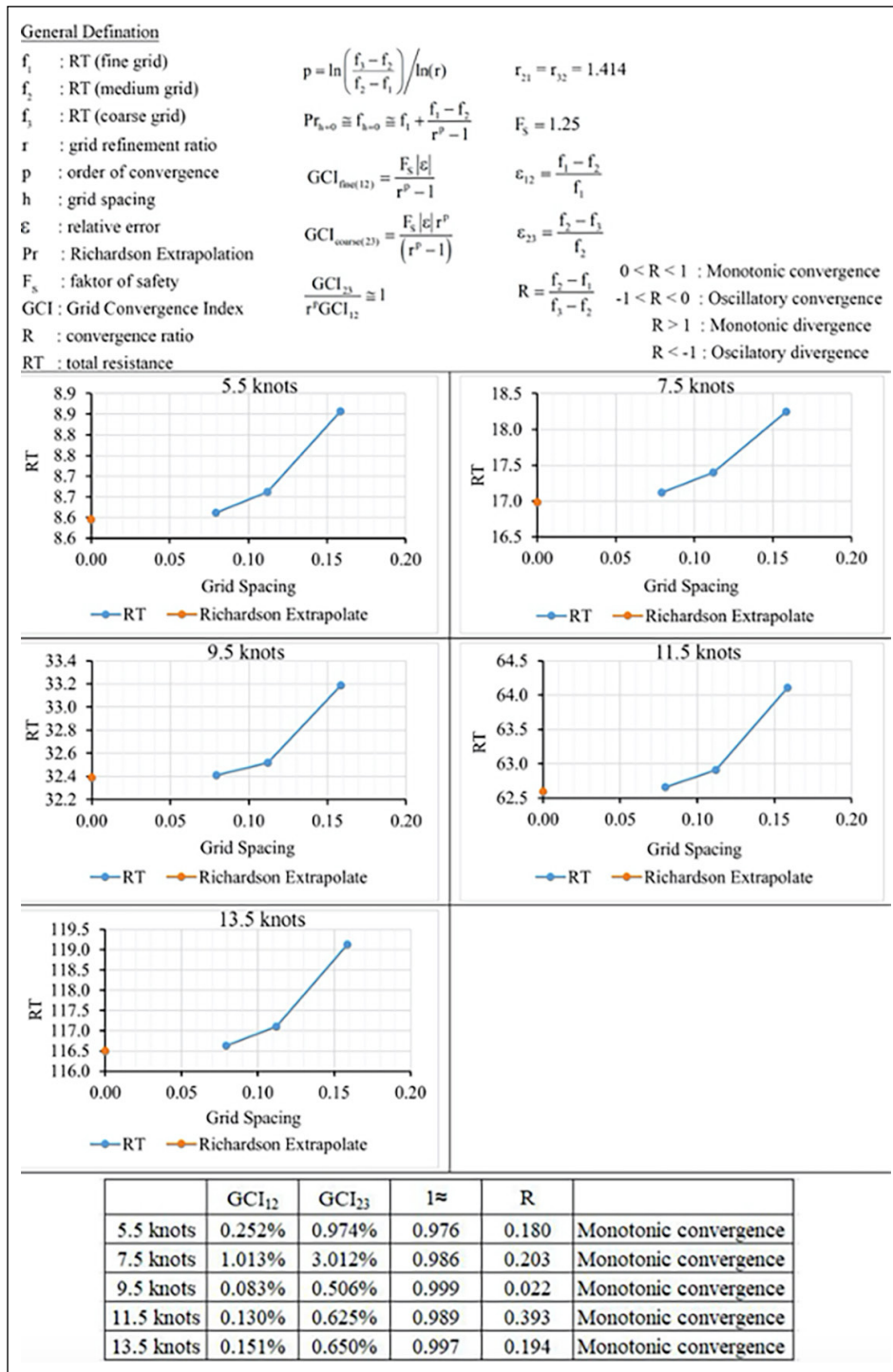


Figure 15. Grid convergence index (GCI) calculations and graphs.

leads to increased wave-making resistance due to less efficient flow dynamics at the bow. Form SB consistently shows lower C_p values than Form WB. This suggests that the addition of a bulbous bow significantly reduces wave-making resistance by altering the wave system and improving flow conditions at the bow. Form SBE exhibits the lowest C_p values for a wide range of F_n values, particularly in the mid-to-high F_n range. This indicates that the special elliptical bulbous bow design is the most effective at reducing wave-making resistance among the forms. Form EB shows moderate C_p values, lower than

Form WB but higher than Form SB and SBE at most F_n values. This suggests that the elliptical bulbous bow is effective but not as optimized as the special elliptical bulbous bow (SBE). At higher F_n values, the differences in C_p become more pronounced, with Form SBE consistently outperforming the other forms. Form WB's C_p increases sharply at higher F_n , highlighting the inefficiency of the bulb-less form in reducing wave-making resistance. At lower F_n values, the C_p differences between the forms are minimal, indicating that bulbous bow design has a lesser impact at lower speeds. In summary, Form SBE is the

Table 6. Results of CFD resistance analysis for form WB

Velocity		Fn	Total resistance	Pressure resistance	Shear resistance	ITTC 1957 (friction correlation)	Effective power (RT*V)
[knots]	[m/s]						
5.5	2.829	0.160	7.842	3.962	3.880	3.784	22.185
7.5	3.858	0.218	16.764	9.806	6.958	6.728	64.676
9.5	4.887	0.277	33.154	22.580	10.574	10.436	162.024
11.5	5.916	0.335	66.694	51.360	15.334	14.890	394.562
13.5	6.944	0.393	118.560	97.340	21.220	20.060	823.281

CFD: Computational Fluid Dynamics; WB: Without Bulb Form; ITTC: The International Towing Tank Conference; RT*V: Total Resistance*Speed.

Table 7. Results of CFD resistance analysis for form SB

Velocity		Fn	Total resistance	Pressure resistance	Shear resistance	ITTC 1957 (friction correlation)	Effective power (RT*V)
[knots]	[m/s]						
5.5	2.829	0.154	8.662	4.670	3.992	3.840	24.505
7.5	3.858	0.210	17.398	10.176	7.222	6.828	67.121
9.5	4.887	0.266	32.518	21.280	11.238	10.594	158.915
11.5	5.916	0.322	62.906	47.160	15.746	15.116	372.152
13.5	6.944	0.378	117.100	95.260	21.840	20.380	813.142

Table 8. Results of CFD resistance analysis for form SBE

Velocity		Fn	Total resistance	Pressure resistance	Shear resistance	ITTC 1957 (friction correlation)	Effective power (RT*V)
[knots]	[m/s]						
5.5	2.829	0.154	8.442	4.424	4.018	3.848	23.882
7.5	3.858	0.209	16.368	9.098	7.270	6.842	63.148
9.5	4.887	0.265	31.852	20.720	11.132	10.618	155.661
11.5	5.916	0.321	64.916	48.820	16.096	15.150	384.043
13.5	6.944	0.377	116.320	94.560	21.760	20.420	807.726

Table 9. Results of CFD resistance analysis for form EB

Velocity		Fn	Total resistance	Pressure resistance	Shear resistance	ITTC 1957 (friction correlation)	Effective power (RT*V)
[knots]	[m/s]						
5.5	2.829	0.160	9.886	5.900	3.986	3.982	27.980
7.5	3.858	0.218	17.816	10.648	7.168	7.076	68.740
9.5	4.887	0.276	32.684	22.180	10.504	10.978	159.700
11.5	5.916	0.335	68.278	52.100	16.178	15.662	404.000
13.5	6.944	0.393	122.840	100.460	22.380	21.100	853.200

most efficient in reducing pressure resistance, particularly at higher Fn values. Form SB is Effective, but slightly less efficient than SBE. Form EB is moderate performance; better than WB but not as optimized as SBE or SB. Form WB is the least efficient, showing the highest C_p values, especially at higher speeds. This graph highlights the effectiveness of bulbous bow designs, especially the special elliptical bulbous bow (SBE), in minimizing wave-making resistance and improving overall hydrodynamic efficiency at higher operational speeds.

As can be seen in Figure 22, across all forms, the C_T increases as the Fn rises. This is expected because, at higher speeds, wave-making resistance and viscous resistance become more significant, contributing to the overall resistance. Form WB consistently shows higher C_T values compared to the other forms, particularly at higher Fn values. This suggests that the absence of a bulbous bow results in higher total resistance, likely due to increased wave-making resistance. Form SB exhibits lower C_T values compared to Form WB. This indicates that the bulbous bow effectively

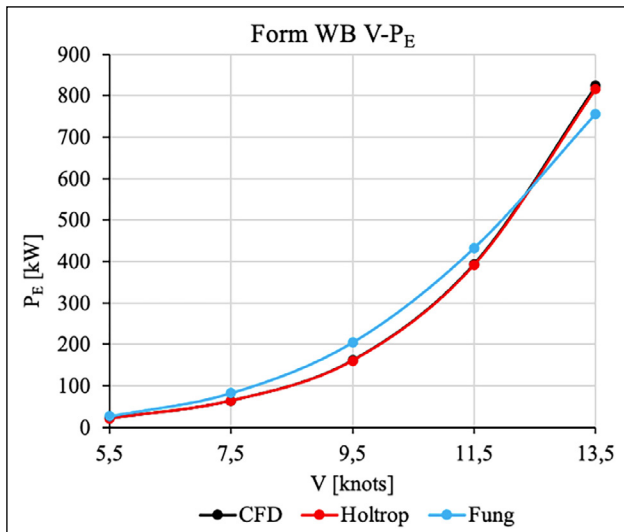


Figure 16. CFD, Holtrop, and Fung effective power curves for Form WB.

CFD: Computational Fluid Dynamics; WB: Without Bulb Form.

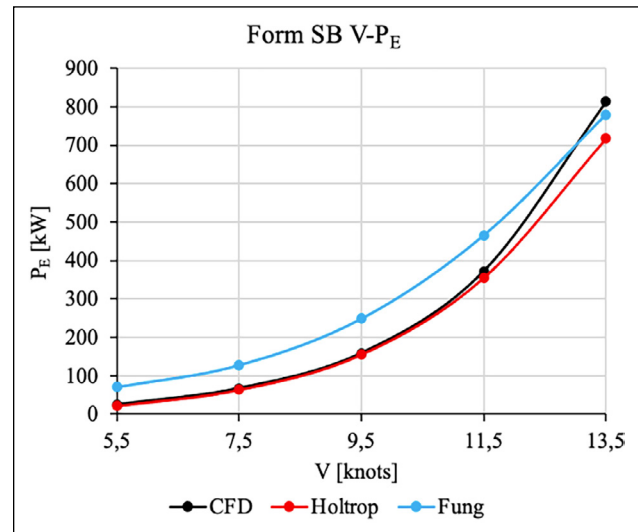


Figure 17. CFD, Holtrop, and Fung effective power curves for Form SB.

SB: Special Bulb Form.

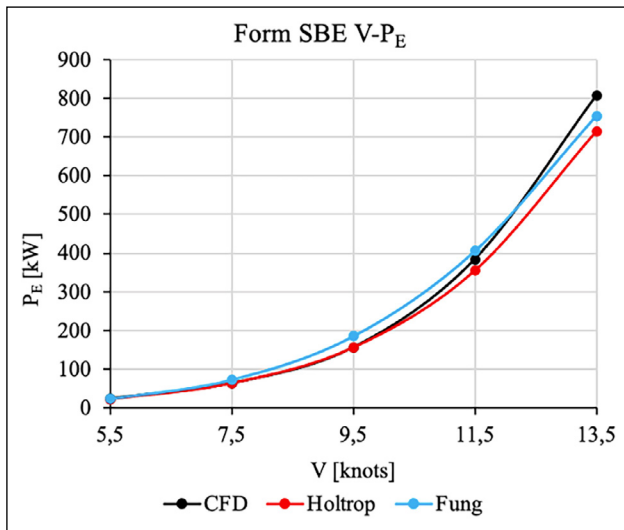


Figure 18. CFD, Holtrop, and Fung effective power curves for Form SBE.

SBE: Special Elliptical Bulb Form.

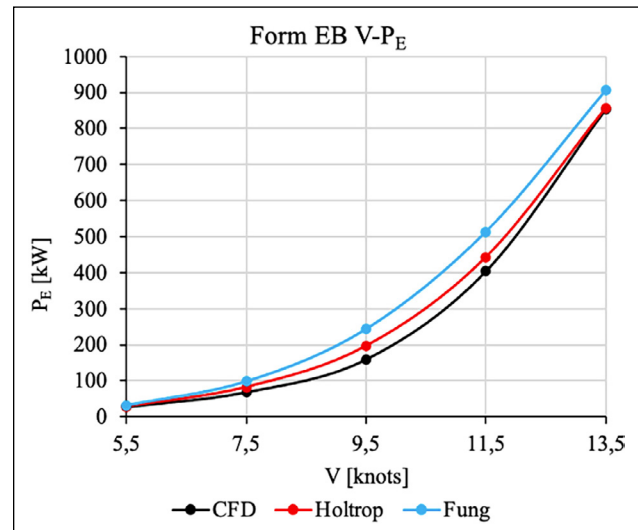


Figure 19. CFD, Holtrop, and Fung effective power curves for Form EB.

EB: Elliptical Bulb Form.

reduces total resistance by improving flow dynamics and reducing wave formation. Form SBE demonstrates the lowest C_T values across most Fn ranges. This suggests that the special elliptical bulbous bow is the most efficient design in minimizing total resistance. Form EB generally shows higher C_T values than Forms SB and SBE, indicating that while the elliptical bulbous bow design is effective, it is not as optimized as the special elliptical design (SBE). At higher Fn values, the difference in C_T values between the forms becomes more pronounced, with Form SBE maintaining the lowest total resistance. At lower Fn values, the differences between the forms are minimal, suggesting that bulbous bow designs have a more significant impact at higher speeds. The efficiency of the bulbous bow designs is clearly evident, with Form SBE consistently outperforming the other forms, followed by Form SB. In summary, Form SBE is the most

efficient in reducing total resistance, especially at higher Fn values. Form SB performs well but slightly less effective than SBE. Form EB is moderately effective; better than WB but not as efficient as SBE or SB. Form WB is the least efficient, with consistently the highest C_T values. This graph highlights the importance of optimized bulbous bow designs, particularly at higher speeds, in reducing total resistance and improving the hydrodynamic performance of the vessel.

Figure 23 illustrates the percentage difference in resistance compared to Form WB across a range of Fn 0.150-0.400 for three different forms: Form SB, Form SBE, and Form EB. The y-axis represents the percentage difference in C_T , where positive values indicate an increase and negative values indicate a decrease in C_T relative to the baseline form. The x-axis represents the Froude number (Fn), which correlates with the vessel's speed.

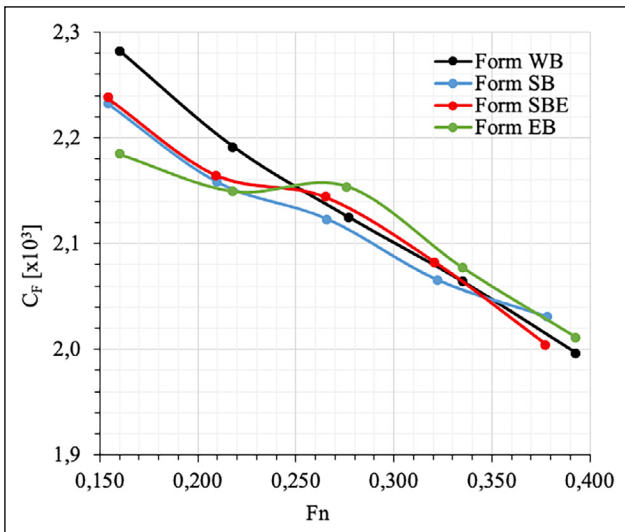


Figure 20. Comparison graph of the coefficients of frictional resistance for the forms.

WB: Without Bulb Form; SB: Special Bulb Form; SBE: Special Elliptical Bulb Form; EB: Elliptical Bulb Form.

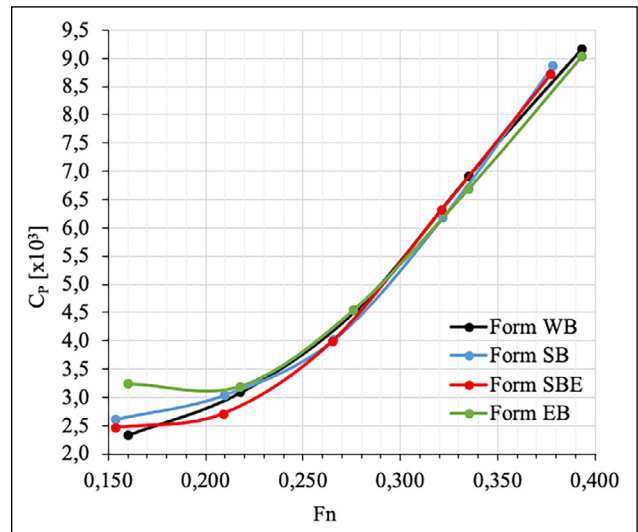


Figure 21. Comparison graph of the coefficients of pressure resistance for the forms.

WB: Without Bulb Form; SB: Special Bulb Form; SBE: Special Elliptical Bulb Form; EB: Elliptical Bulb Form.

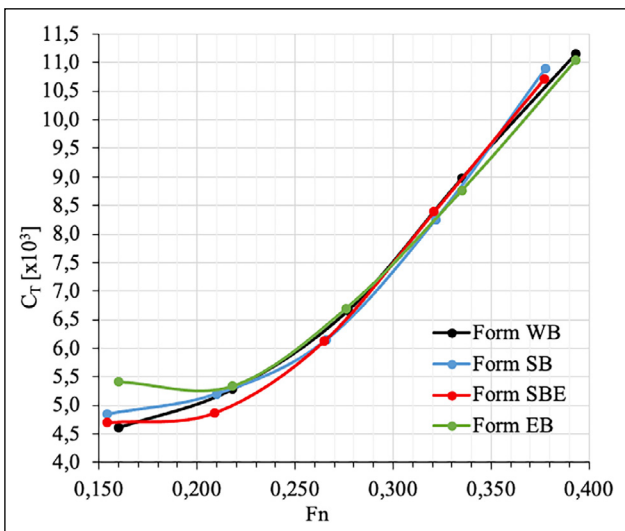


Figure 22. Comparison graph of the coefficients of total resistance for the forms.

When analyzing the changes in C_T of Form SB compared to Form WB, the following conclusions are reached: At lower F_n values, Form SB initially exhibits a slight increase in resistance compared to Form WB. As F_n increases (around 0.2–0.3), the resistance begins to decrease, reaching a negative peak (indicating a reduction in resistance) at around $F_n=0.25$. At higher F_n values ($F_n>0.35$), resistance increases sharply, making this form less efficient at higher speeds.

When analyzing the changes in C_T of Form SBE compared to Form WB, the following conclusions are reached: Form SBE shows the largest resistance reduction at mid-range F_n values, peaking around $F_n=0.215$ with a percentage decrease of approximately -5%. It maintains a consistent reduction in resistance across most F_n values, demonstrating good performance. At higher F_n values ($F_n>0.35$), resistance begins to slightly increase, though the increase is less pronounced compared to Form SB.

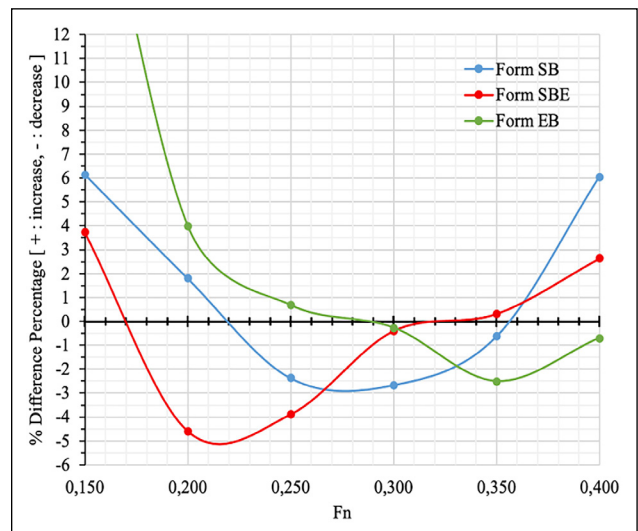


Figure 23. The percentage changes in C_T values of Forms SB, SBE, and EB compared to Form WB.

When analyzing the changes in C_T of Form EB compared to Form WB, the following conclusions are reached: At lower F_n values, Form EB shows a significant increase in resistance, likely due to suboptimal performance of the elliptical bulbous bow at low speeds. As F_n increases, the resistance stabilizes and becomes comparable to the baseline form at around $F_n=0.3$. Form EB shows the largest resistance reduction at F_n 0.30 values, peaking around $F_n=0.35$ with a percentage decrease of approximately -2.5%. At higher F_n values, the resistance begins to increase again, though less sharply than Form SB.

Form SBE demonstrates the best performance in reducing resistance, particularly in the mid- F_n range (0.2–0.3), where it consistently achieves the largest percentage decrease. This makes it the most efficient design for moderate-speed operations. In contrast, Forms SB and EB perform less efficiently at higher F_n

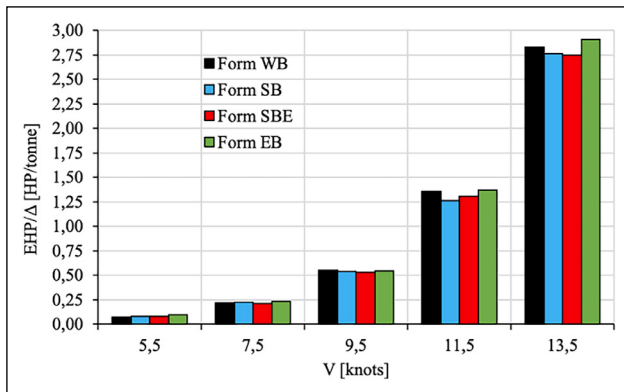


Figure 24. Values of the EHP/Δ (effective power/displacement tonnage) ratio for the speeds.

WB: Without Bulb Form; SB: Special Bulb Form; SBE: Special Elliptical Bulb Form; EB: Elliptical Bulb Form; EHP: Effective Horsepower.

values, as their resistance percentages increase relative to the baseline. Additionally, Form EB shows the poorest performance at low Fn values, likely due to its design being less suited to slower speeds.

Form SBE proves to be the most efficient design for reducing resistance, particularly in the mid-range Fn values, making it highly suitable for moderate speeds. Form SB demonstrates moderate performance but becomes less effective at higher speeds, while Form EB struggles at lower speeds, stabilizing in the mid-Fn range before showing a slight increase in resistance at higher Fn values. This analysis underscores the importance of tailoring bulbous bow designs to the vessel's operational speed range to achieve optimal hydrodynamic performance.

In Figure 24, the EHP/Δ (effective power per displacement ton) ratios of the forms are compared based on their velocities. The effective power per ton was calculated for each speed. At 5.5 knots, Form EB exhibited the worst performance, while the other forms performed almost identically. At 7.5 knots, Form SBE achieved the best performance, whereas Form SB performed the worst. At 9.5 knots, Form SBE emerged as the optimal form, while Form WB showed the poorest performance. At 11.5 knots, Form SB delivered the best performance, with Form EB being the least efficient. Finally, at 13.5 knots, Form SBE again demonstrated the best performance, while Form EB showed the worst. Overall, Form SBE consistently demonstrated the best performance, except at speeds of 5.5 and 11.5 knots.

7. CONCLUSION

This study investigated the hydrodynamic performance of various bow forms, including bulbous bow designs, on a typical Black Sea fishing vessel using Computational Fluid Dynamics (CFD) analyses. The primary objective was to evaluate the effectiveness of different bulbous bow shapes in reducing total resistance across a range of operational speeds. Four forms were analyzed: the baseline bulb-less form (Form WB), the conventional bulbous bow form

(Form SB), the special elliptical bulbous bow form (Form SBE), and the elliptical bulbous bow form (Form EB).

The results revealed that the bulbous bow designs significantly influence the total resistance of the vessel, with the special elliptical bulbous bow (Form SBE) consistently demonstrating the best overall performance. Form SBE exhibited the lowest effective power per displacement tonnage (EHP/Δ) and reduced wave heights at higher speeds, particularly in the critical speed range of 9.5 to 13.5 knots, where wave-making resistance becomes dominant. The conventional bulbous bow form (Form SB) also performed well but was less efficient than Form SBE at higher speeds. The elliptical bulbous bow form (Form EB) showed moderate performance, especially at lower speeds, while the bulb-less form (Form WB) had the highest resistance values across all speed ranges.

A key observation was the relationship between speed and the effectiveness of the bulbous bow designs. At lower speeds, frictional resistance dominated, reducing the impact of bulbous bows. However, at higher speeds, where wave-making resistance is significant, the optimized bulbous bow designs effectively reduced total resistance and smoothed wave patterns along the hull.

This study underscores the importance of tailored bulbous bow designs for specific vessel types and operational profiles. For Black Sea fishing vessels, the special elliptical bulbous bow (Form SBE) is recommended as the optimal solution for minimizing resistance and enhancing efficiency. Future research could focus on validating these results through experimental towing tank tests and exploring the performance of these designs under varying sea conditions.

ACKNOWLEDGEMENTS

The authors gratefully acknowledge the high-speed computing laboratory of Naval Architecture and Marine Engineering Department, Karadeniz Technical University.

DATA AVAILABILITY STATEMENT

The published publication includes all graphics and data collected or developed during the study.

CONFLICT OF INTEREST

The author declared no potential conflicts of interest with respect to the research, authorship, and/or publication of this article.

ETHICS

There are no ethical issues with the publication of this manuscript.

USE OF AI FOR WRITING ASSISTANCE

No AI technologies utilized.

FINANCIAL DISCLOSURE

The authors declared that this study has received no financial support.

REFERENCES

- Abramowski, T., & Sugalski, K. (2017). Energy saving procedures for fishing vessels by means of numerical optimization of hull resistance. *Zeszyty Naukowe Akademii Morskiej w Szczecinie*, 49(121), 19–27.
- Atlar, M. (1977). *Investigation the effect of scale and bulbous bow on the fishing boats* [Unpublished master thesis]. Istanbul Technical University. [Turkish]
- Baba, E. (1969). A new component of viscous resistance of ships. *Transactions of the Society of Naval Architects of Japan*, 125, 69–81. [CrossRef]
- Başaran Gemi. *Eminoğulları 3*. <https://www.basarangemi.com.tr/ships/balik-avci/eminogullari-3> Accessed on Nov 01, 2024.
- Başaran Gemi. *Habibin Yavuz*, <https://www.basarangemi.com.tr/ships/balik-avci/habibin-yavuz> Accessed on Nov 01, 2024.
- Başaran Gemi. (2024). Hakkımızda, başaran gemi sanayi. <https://www.basarangemi.com.tr/pages/hakkimizda> Accessed on Nov 01, 2024.
- Bahatmaka, A., & Kim, D. J. (2019). Numerical approach for the traditional fishing vessel analysis of resistance by CFD. *Journal of Engineering Science and Technology*, 14(1), 207–217.
- Bragg, M. (1930). Results of experiments upon bulbous bows. *Transactions SNAME*, 38, 13–43.
- CD-Adapco. (2014). User Guide, Star-CCM+ Version 9.04, CD-Adapco.
- Díaz-Ojeda, H. R., Pérez-Arribas, F., & Turnock, S. R. (2023). The influence of dihedral bulbous bows on the resistance of small fishing vessels: A numerical study. *Ocean Engineering*, 281, Article 114661. [CrossRef]
- Díaz Ojeda, H. R., Oyuela, S., Sosa, R., Otero, A. D., & Pérez Arribas, F. (2024). Fishing vessel bulbous bow hydrodynamics-a numerical reverse design approach. *Journal of Marine Science and Engineering*, 12(3), Article 436. [CrossRef]
- Dinçer, A. C. (1992). *A design study of Turkish Black Sea fishing vessels [Master thesis]*. University of Glasgow. Available from ProQuest Dissertations & Theses Global database. (UMI No. 11011427).
- Ergün Gemi. (2024). *Kurumsal tarihçe*. <https://ergungemi.com.tr/hakkimizda/> Accessed on Nov 01, 2024.
- Ferguson, A. M. (1967). Hull and bulbous bow interaction. *Transactions RINA*, 112(4), 421–441.
- Inui, T., Takaehi, T., & Kumano, M. (1960). Wave profile measurement on the wave making characteristics of the bulbous bow. Society of Naval Architects of Japan (Translation from the University of Michigan), 16–35. [CrossRef]
- Inui, T. (1962). Wave making resistance of ships. *Transactions SNAME*, 70, 283–313.
- Iqbal, M., Budiarto, U., Hidayat, K. Z., Hernanta, H. H., & Trimulyono, A. (2021). The influence of foil-shaped center bulb geometry into catamaran fishing vessels resistance. In *IOP Conference Series: Materials Science and Engineering*, 1034(1), IOP Publishing.
- ITTC. (2021). *ITTC-Recommended Procedures and Guidelines: Uncertainty analysis in CFD verification and validation methodology and procedures*. Eff. Date 2021, Revision 04.
- Kafalı, K., Şaylan, O., & Salcı, A. (1979). *Developing of hull forms of fishing boats suitable for Turkish waters*. The Scientific & Technological Research Council of Turkey, Project No. G-416. [Turkish]
- Kim, D.J., Iqbal, M., Bahatmaka, A., & Prabowo, A. R. (2018). *Bulbous bow applications on a catamaran fishing vessel for improving performance*. In: MATEC Web of Conferences, 159, (1-6), EDP Sciences. [CrossRef]
- Kracht, A. M. (1978). Design of bulbous bows. *Transactions SNAME*, 86, 197–217.
- Li, C., Wang, Y., Chen, J. (2016). *Study on the shape parameters of bulbous bow of tuna longline fishing vessel*. 5th International Conference on Energy and Environmental Protection (ICEEP 2016), 17-18 September 2013, (250–255). Shenzhen. [CrossRef]
- Muntjewerf, J. J. (1967). Methodical series experiments on cylindrical bows. *Transactions RINA*, 112(2), 199–223.
- Oyuela, S., Ojeda, H. R. D., Arribas, F. P., Otero, A. D., & Sosa, R. (2024). Investigating fishing vessel hydrodynamics by using EFD and CFD tools, with focus on total ship resistance and its components. *Journal of Marine Science and Engineering*, 12(4), Article 622. [CrossRef]
- Özdemir, Y., H. (2007). *Investigation of the flow surrounding the ship by using computational fluid dynamics [Master thesis]*. Yıldız Technical University. Council of Higher Education Thesis Center (Accession No. 213256). [Turkish]
- Raju, M.S.P., Sivabalan, P., Thamby, T., & Saravanan, B. (2020). Effect of bulbous bow on resistance of a tuna longliner. *International Journal of Advanced Research in Engineering and Technology*, 11(2), 136–145.
- Roache, P., J. (1994). Perspective: a method for uniform reporting of grid refinement studies. *Journal of Fluids Engineering*, 116(3), 405–413. [CrossRef]
- Richardson, L. F. (1927). The deferred approach to the limit. *Transactions of the Royal Society of London, Series A*, 226, 299–361. [CrossRef]
- Samuel, S., Iqbal, M., Utama, I.K.A.P. (2015). An investigation into the resistance components of converting a traditional monohull fishing vessel into catamaran form. *International Journal of Technology*, 6(3), 432–441. [CrossRef]
- Saral, D. (2016). *A systematic investigation of the effects of various bulbous bows on resistance of fishing boats [Master thesis]*. Karadeniz Technical University. Council of Higher Education Thesis Center (Accession No. 430371). [Turkish]
- Saral, D. (2023). *Form optimization of the Black Sea type fishing vessels [Doctorial Thesis]*. Karadeniz Technical University. Council of Higher Education Thesis Center (Accession No. 791295). [Turkish]

- Saral, D., Aydın, M. & Köse, E. (2018). A systematic investigation of the effects of various bulbous bows on resistance of fishing boats. *Brodogradnja*, 69(2), 93–117. [\[CrossRef\]](#)
- Saral, D. & Köse, E. (2020). Resistance analyses of a traditional Black Sea type fishing ship with CFD in calm water. *Turkish Journal of Maritime and Marine Sciences*, 6(2), 207–223.
- Saral, D., & Köse, E. (2024). Academic studies on fishing vessels in Turkey. *Ocean Engineering*, 308, Article 118295. [\[CrossRef\]](#)
- Setyawan, D., Utama, I. K., Murdijanto, M., Sugiarto, A., & Jamaluddin, A. (2010). Development of catamaran fishing vessel. *IPTEK The Journal for Technology and Science*, 21(4), 167–173. [\[CrossRef\]](#)
- Sharma, R., & Sha, O. P. (2005). Practical hydrodynamic design of bulbous bows for ships. *Naval Engineers Journal*, 117(1), 57–75. [\[CrossRef\]](#)
- Shearer, J. R., & Steele, B. N. (1970). Some aspects of the resistance of full form ships. *Transactions RINA*, 112(4), 69–83.
- Shih, T. H., Liou, W. W., Shabbir, A., Yang, Z., & Zhu, J. (1995). A new $k-\epsilon$ Eddy-viscosity model for high Reynolds number turbulent flows-model development and validation. *Computers Fluids*, 24(3), 227–238. [\[CrossRef\]](#)
- Siemens. (2021). *User Guide, Simcenter STAR-CCM+ Hull Performance Workflow 2021.2*.
- Söylemez, M. (1983). *Application of bulb to fishing boats* [Undergraduate Graduation Project]. Istanbul Technical University. [Turkish]
- Szelangiewicz, T., Abramowski, T., Żelazny, K., & Sugalski, K. (2021). Reduction of resistance, fuel consumption and GHG emission of a small fishing vessel by adding a bulbous bow. *Energies*, 14(7), Article 1837. [\[CrossRef\]](#)
- Taylor, D. W. (1923). *Marine Engineering and Shipping Age* (pp. 540–548). Aldrich Publishing Company.
- Tran, T. G., Van Huynh, C., & Kim, H. C. (2021). Optimal design method of bulbous bow for fishing vessels. *International Journal of Naval Architecture and Ocean Engineering*, 13, 858–876. [\[CrossRef\]](#)
- Weinblum, G. (1935). Die theorie der wulstschiffe. *Der Gesellschaft für Angewandte Mathematik*, 135–156.
- Wigley, W. C. S. (1936). The theory of bulbous bow and its practical application. *Transactions NECIES*, 52, 65–88.
- Yim, B. (1963). On ships with zero and small wave resistance. Paper presented at the in Proceedings of International Seminar on Theoretical Wave Resistance, Michigan, USA, 163–193. [\[CrossRef\]](#)
- Yim, B. (1965). Analyses of spherical bulbs on a ship bow. Inc. *Technical Report 117*, 28–39.
- Yim, B. (1974). A simple design theory and method for bulbous bows of ships. *Journal of Ship Research*, 18 (3), 141–152. [\[CrossRef\]](#)
- Yim, B. (1980). Simple calculation of sheltering effect on ship-wave resistance and bulbous bow design, *Journal of Ship Research*, 24 (4), 232–243. [\[CrossRef\]](#)